J. Fluid Mech. (2006), *vol.* 550, *pp.* 61–83.
doi:10.1017/S0022112005007858 Printed in the United Kingdom

Exploration of vortex dynamics for transitional flows in a three-dimensional backward-facing step channel

By TONY W. H. SHEU AND H. P. RANI

Department of Engineering Science and Ocean Engineering,
National Taiwan University, Taipei, Taiwan, 106
twhsheu@ntu.edu.tw

(Received 18 January 2005 and in revised form 4 August 2005)

The eddy structures and their mutual interactions in a three-dimensional channel with a backward-facing step for the transitional Reynolds number 900 were investigated numerically. The aim was to reveal the structural development of the entire vortical flow field, which could immensely enhance the knowledge about vortical structures occurring in the recirculation region near the step wall. Simulations were made to reproduce the experimental observations and provide clear indications about the strong interaction between the shear layer instabilities. Physical instabilities of this type were amplified by the shedding-type instabilities and induced by the interaction of coherent structures with the sidewalls of the duct. These interactions were responsible for the flapping motion of interior shear layer. Careful attempts were made to reveal the behaviour of these vortical structures by means of vortex stretching, roll-up of vortex lines and formation of vortex tubes. Also, the three-dimensional flow topology of the velocity field corresponding to stationary helical vortex (SHV) was analysed extensively. The SHV flow consisted of a pair of counter-rotating helical cells in a double helix structure wrapped around the vortex tube. The roll-up shear-layer hovering vortices were observed near the step to initiate the Kelvin–Helmholtz-like instability. The Kelvin–Helmholtz vortices were developed into lambda-shaped vortices which impinged on the step-wall and were elongated into the hairpin-like vortices.

1. Introduction

Study of flow separation and its subsequent re-attachment to solid surfaces in a backward-facing step flow has attracted many investigators owing to its importance to various engineering disciplines. In this channel flow, only one major separation region that is located near the step is observed. After the separation, the flow slowly moved towards an equilibrium turbulent boundary layer. Under such circumstances, it was necessary to carry out detailed numerical simulations for exploring the flow physics embedded in this model and to compare the prediction and benchmark solutions to validate the accuracy. For the last three decades, both two-dimensional and three-dimensional backward-facing step expansion flows have been studied experimentally and analytically for meeting the challenges of practical applications.

As a benchmark for two-dimensional numerical simulations, the backward-facing step has been the subject of experimental (Armaly *et al.* 1983; Kosma 2000; Lee, Huteau & Mateescu 2000) and numerical investigations (Guerrero & Cotta 1996;

Koutmos & Mavridis 1997; Choi, Hinze & Kunisch 1999). Recently, the two-dimensional simulation studies of Dejoan & Leschziner (2004) in the periodically perturbed flow over a backward-facing step identified the involvement of both shear-layer and shedding-type instabilities in the promotion of reattachment. Beaudoin *et al.* (2004) in their three-dimensional backward-facing step flow study have observed the presence of longitudinal vortices. They concluded that the instability originated from the vicinity of the reattached flow. They argued that their experiment was the first one to show a spanwise periodicity of the flow. Also the critical-Reynolds-number effect on the flow behaviour of the three-dimensional backward-facing step flow was studied by Nie & Armaly (2004). They concluded that the flows with a Reynolds number Re value of less than 400 are of the laminar flow type, Re falling between 400 and 3400 could, however, yield transitional flows. Turbulent flow was observed for the case with Re above 3400.

Several experimental and numerical investigations have been performed to increase our understanding of the stability criteria regarding the recirculation phenomena and critical Re in backward-facing step flow. In recent times, studies have also been focused on the generation and deformation of the three-dimensional vortical structures and characterization of unsteady coherent structure in this channel. The flow field in the backward-facing step channel can be divided into three regions: (i) the flow near the step, (ii) the separated region, and (iii) the free shear layer which is located on the lee side of the downstream and is characterized by its large velocity gradient. Thus, an accurate presentation of the detailed vortex dynamics of this flow is a challenging task.

Yanase, Kawahara & Kiyama (2001) have examined the generation of three-dimensional vortical structures in a backward-facing step channel at $Re = 700$. They revealed that these three-dimensional structures first appeared through the three-dimensional deformation of a row of spanwise vortices owing to the linear translational instability of the flow. Similar results were obtained by Pierrehumbert & Windal (1982). Yanase *et al.* (2002) noticed that the deformed three-dimensional vortices were connected with each other by rib structures with a strong streamwise vorticity that led to the generation of a staggered array of the streamwise vortices. These streamwise vortices induce the formation of streamwise vortex tubes of alternating signs in near-wall turbulence. Kiya & Sasaki (1985) studied the formation of a three-dimensional hairpin vortical structure in the reattaching region of this duct flow. Jeong *et al.* (1997) identified these coherent structures as one of the most remarkable flow structures. These three-dimensional structures were developed into a staggered array of quasi-streamwise vortices. These three-dimensional coherent structures differ from the two-dimensional ones by means of vortex stretching (Majda 1991; Zhou 1997). Gallaire (2002) noticed that this complex three-dimensional phenomenon depended on the flow circulation and Re. Gupta, Lilley & Syred (1984) observed that a large recirculation zone with high reversed flow velocities could lead to vortex breakdown.

Earlier studies tried to understand the instabilities and vortex structures in the recirculation region of the three-dimensional backward-facing step flow, but we still require understanding of the interaction of vortex structures in this region. Hence, an attempt has been made in this study to analyse numerically the interaction of vortex structures in the three-dimensional backward-facing step flow. The main objective of the present study that followed the experimental investigations of Nie & Armaly (2004) was to investigate the three-dimensional vortical structure within the separated and reattached region with emphasis on the exploration of the

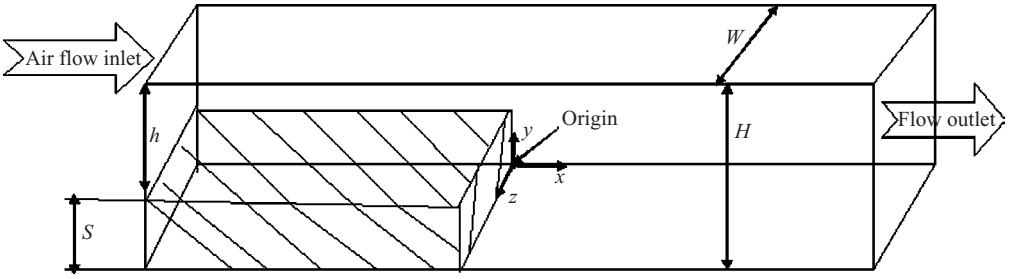

FIGURE 1. Schematic of the backward-facing step flow problem under current investigation.

coherent structure. Therefore, the current direct numerical simulation (DNS) study was carried out corresponding to the flow and model conditions of the experimental study. The numerical results, however, provided complete knowledge of the three-dimensional velocity $\overline{V} = (u, v, w)$ and vorticity $\overline{\omega} = (\omega_x, \omega_y, \omega_z) = \nabla \times \overline{V}$ fields, which were difficult to obtain from experiments. The investigation of the nonlinear interactions was restricted by the simplification of equations and by the accuracy of the corresponding numerical methods used.

Let us begin in § 2 with a detailed description of the computational model along with the conservation laws for mass and momentum of the incompressible fluid flow that was investigated. This will be followed in § 3 with the details about grid generation and numerical methods for solving the Navier–Stokes equations subject to the proper initial and boundary conditions. In § 4 the three-dimensional transitional 'flapping' flow topology in the recirculation zone is explained in detail with the help of limiting streamlines, velocity contours and spectral analysis. Corroborative evidence for the proposed SHV streamline is provided by invoking topological constraints, structural stability criteria and listing the experimental evidence. The presence of Kelvin–Helmholtz instability caused by the interior shear layers and spanwise instability due to the shedding eddy is highlighted. Also, the three-dimensional coherent structure is elucidated with the aid of vortex lines, vortical corelines and vortex tubes extracted from the simulated velocity data and finally, of course, concluding remarks are made.

2. The simulated flow conditions

A three-dimensional air flow in a duct with a backward-facing step is schematically presented in figure 1. The origin of the coordinate system is at the bottom corner of the step. Air arrives from an inlet channel of height 0.98 cm (h) and flows downstream into an outlet channel of height 1.98 cm (H). The upstream and downstream width of the duct was chosen as 8 cm (W). This geometry consisted of a backward-facing step of height S ($= 1$ cm), expansion ratio ER ($= H/(H - S) = 2.02$) and an aspect ratio AR ($= W/S = 8$). The duct lengths of current interest were chosen as 100 cm and 50 cm in the upstream and downstream of the step, respectively. The physical domain of length $-100 \leqslant x/S \leqslant 50$ was considered to avoid the significant sudden expansion flow at the step. We observed that an increase in the downstream length ($x/S > 50$), however, did not change the flow behaviour. To corroborate this, the length of the downstream computational domain was increased to $x/S = 75$. The flow behaviour at $x/S = 50$ and $x/S = 75$ showed the same set of results. Therefore, it was confirmed that the use of a longer computational domain did not change the flow in the region downstream from the step. Hence the downstream length of $x/S = 50$ was sufficient for further analysis. The following continuity equation along with the

Total number of cells	233 136	105 656	52 928
u ($\mathrm{m\,s^{-1}}$)	1.15767	1.15769	1.14738

TABLE 1. Grid independence test.

three-dimensional Navier-Stokes equations have been employed for an incompressible viscous fluid passing through a backward-facing step:

$$\nabla \cdot \overline{V} = 0, \tag{1}$$

$$\frac{\partial \overline{V}}{\partial t} + (\overline{V} \cdot \nabla)\overline{V} = -\nabla P + \frac{1}{Re}\nabla^2 \overline{V}. \tag{2}$$

In the above working equations, $\overline{V}$, P and t represent the velocity vector, pressure and time, respectively. The Reynolds number Re is given by $\rho u_0 D_h/\mu$, where $D_h = 2Wh/(W + h)$ and u_0 is the average inlet velocity according to the work of Nie & Armaly (2004). In the following sections, the velocity components u, v and w are referred to as the streamwise, transverse and spanwise velocities, respectively.

3. The computational procedures and the generated mesh

The three-dimensional backward-facing step flow was analysed using well-developed commercially available software, namely, CFDRC (CFD Research, Huntsville, AL, USA), for gaining the physical insight. In the first analysis phase, the geometry of the flow model was constructed using the grid-generation software, namely, CFD-GEOM. The non-uniform grids were generated and clustered in the vicinity of bounding walls and near the step. The total number of grids used in the present study was 105 656. The flow volume, boundary and initial conditions for this model had been provided in the CFD-ACE solver. The values of the air density (ρ) and dynamic viscosity (μ) were fixed as $1.23\,\mathrm{kg\,m^{-3}}$ and $1.78 \times 10^{-5}\,\mathrm{kg\,m^{-1}\,s^{-1}}$. The upwind numerical method for spatial derivatives was used. The Euler first-order time-marching solution was obtained for the unsteady calculations at the time step of 0.01 s. The number of steps employed in current transient studies was 1035. These time steps were felt to be sufficient to ensure the transitional behaviour of the present study and to resolve the low-frequency flow features to reach a state that is independent of the initial condition. The flow was, however, assumed to start from rest. No-slip boundary conditions were imposed on the walls. Zero-gradient boundary conditions were assumed at the exit section of the duct ($x/S = 50$). The algebraic multigrid method was used as a means of acceleration. In all the investigations, the iterative calculations of the primitive variables, such as pressure and velocity, were terminated when the residual norm criteria reached $\leqslant 10^{-9}$. In the final stage, the predicted results were viewed and analysed by the three-dimensional animated plotting tools such as the CFD-VIEW and TecPlot.

The mesh density has been varied so that the computed solutions represent the real flow physics. A series of grid independence tests was conducted to determine the optimal mesh. The solution obtained through the grid size (0.035, 0.03, 0.1) was found to be closer to the experimental results of Nie & Armaly (2004). Hence, in the present analysis, the above grid size was selected as the optimal mesh.

Table 1 shows the quantitative information for the grid independence test at a point (−10, 1.49, 4). When the currently employed number of cells 105 656 was increased by 50 %, the solution did not vary much and the discrepancy is observed only at the fourth decimal place. When the cells are reduced by 50 %, the solution varied, however,

in the second decimal place. Hence, in the currently employed calculations, 105 656 cells are used. Though it was possible that the finer meshes would yield more accurate results, the insufficient computational resources did not allow further refinement.

4. Results and discussion

We begin by presenting the flow topology to give a global picture of the three-dimensional flow development in the backward-facing step channel. In the following sections, all the results are presented and discussed for the flow considered at $Re = 900$, which lies very close to the transitional regime (Nie & Armaly 2004). To obtain an understanding of the three-dimensional character of the flow structure, we may resort to the topology of limiting streamlines or skin friction lines in order to extract meaningful flow physics from an enormous amount of computed data. In this paper, the limiting streamlines defined as the streamlines passing very close to the solid wall were chosen to depict the flow structure. By making use of the kinematic nature of limiting streamlines, we classified the critical points as singular nodes, foci and saddles. Figure 2 shows the streamlines along the symmetry plane and limiting streamlines adjacent to the step wall, channel roof, floor and vertical endwall. This illustration would help us to visualize the global structure of the vortical flow. In figure 2, the saddle points on the roof, floor and symmetry plane are presented. Lines passing through this saddle point are referred to as the attachment and separation lines. On the floor plane, the attachment and separation lines along with the saddle points (highlighted in circles) are shown. These attachment and separation lines appeared to be the barriers in the flow field. Along with these two critical lines, the sign of the direction of the flow has changed: one flow points towards the saddle while the other one points away from the saddle. Another two spiral nodes are seen at the symmetry plane. These nodes are, hereinafter, referred to as the periodically produced hovering vortices, which are present below the separated shear layer. These hovering vortices play a critical role in the formation of Kelvin–Helmholtz instability and will be discussed at length in the following sections. Beyond the reattachment region, no vortices appear to exist, and the only trace of the periodicity is the undulation of the streamlines. The flow upstream of the step plane (figure 2) is found to be divided into two regions in the downstream vicinity of the step wall. The region within the lines of separation and reattachment hereinafter referred to as the reattachment region was our main interest in the present study. The flow physics in this recirculation zone is discussed in detail in the following sections.

4.1. *Recirculation zone*

Computational study was carried out for obtaining the streamwise velocity component adjacent to the bounding walls and downstream from the step wall for the purpose of locating the boundaries of the reversed flow regions. These calculations were used to identify the mean axial locations (x) on these planes where streamwise velocity magnitudes were zero. These lines were also used to locate positions where the axial shear stress component was zero. The separation flow was characterized by the presence of the recirculation zone developed at the downstream side of the step wall.

The separated shear layer and its 'flapping motion' on the symmetry plane are defined by the zero shear stress lines illustrated in figure 3(a). This figure shows the formation of a shedding eddy that oscillates with time in regions close to the step plane. This oscillatory phenomenon is further confirmed from figure 3(b), which depicts the oscillatory motion of the reattachment line on the floor. Along with the reattachment line, the flow shows a periodic behaviour with the reattachment length increasing and

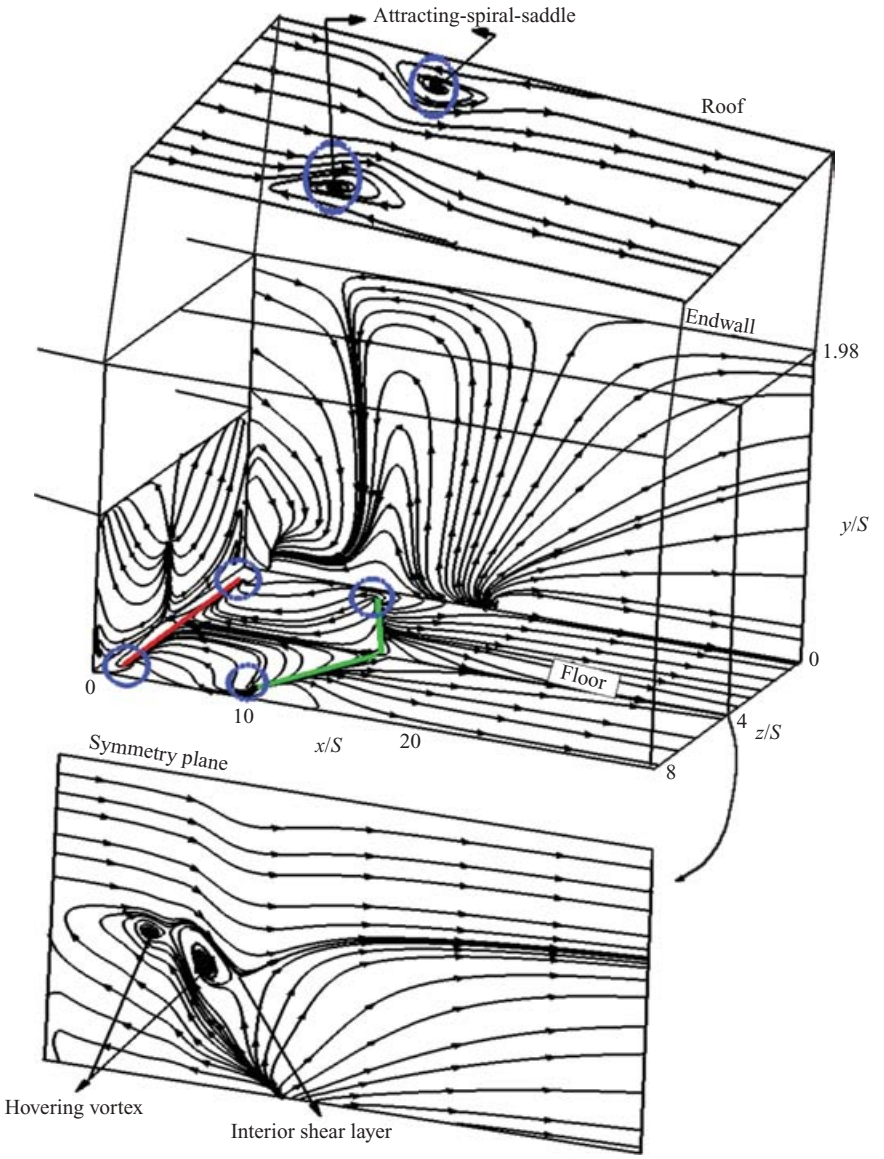

FIGURE 2. The simulated streamlines plotted at the symmetry plane ($z/S = 4$) and the limiting streamlines plotted on the step, vertical endwall, roof and floor of the channel for the case investigated at $Re = 900$ at an instantaneous time $t = 10.35$ s. Note that green line, red line and blue circle denotes the line of separation, line of reattachment and saddle point, respectively.

decreasing. This constant oscillatory behaviour is closely coupled with the vortical structures. From the 'flapping motion', it is observed that the large-scale structures remain in contact with the vertical endwalls for small distance before suddenly detaching from the wall and causing an abrupt upstream shift of the reattachment line. This type of detachment of unsteady structures in the reattachment region coincides with Husan (1992). The period of this fluctuation corresponds to the time required for the large-scale vortices emerging from the step wall to travel downstream and to interact with the vertical endwalls. These are associated with the low-frequency

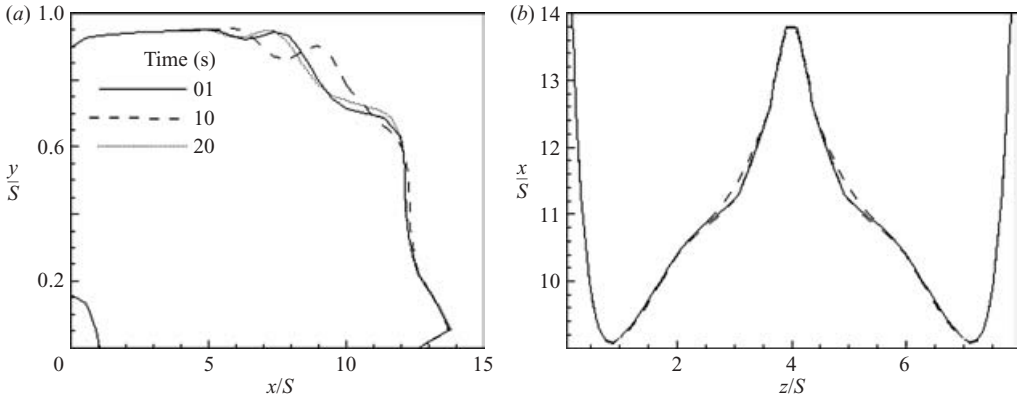

FIGURE 3. The simulated zero shear-stress lines at various times illustrate the 'flapping motion' along the (*a*) symmetry plane ($z/S = 4$) and (*b*) downstream side of the channel floor ($y/S = 0.05$).

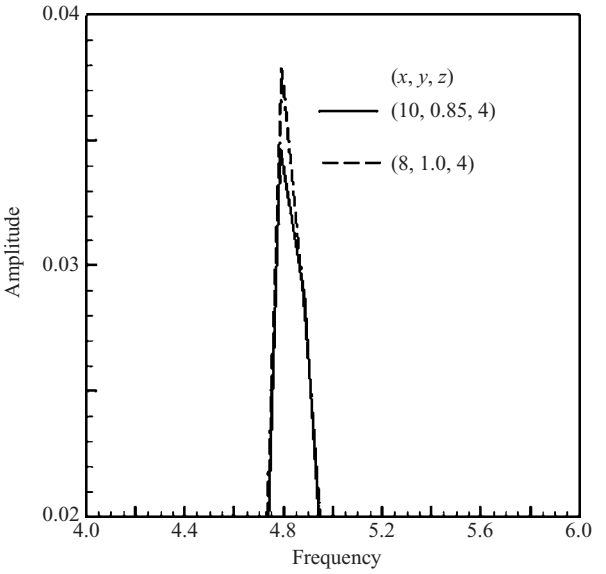

FIGURE 4. The simulated streamwise velocity power spectr*a* at the two chosen points.

'flapping' motion of the shear layer, also referred to as the shedding-type instability (Kiya, Shimizu & Mochizuki 1997). This motion reflects the interaction of the entire shear layer with the vertical endwalls.

Figure 4 demonstrates the spectrum of the streamwise velocity fluctuations along the shear layer at $x/S = 8$ and 10. Fast Fourier transformation averaging procedure was used to obtain the spectrum. The power spectrum features a peak located at the frequency ($f = 4.79$) with amplitude 0.0379. As the flow progresses from the separation point, the frequency corresponding to the peak, $f = 4.79$, shifts towards the lower values. It is observed that this low-frequency mode value is directly linked to the large-scale vortices present in the downstream side of the reattachment region. Further downstream at $x/S = 10$, figure 4 exhibits a low-frequency peak at $f = 4.77$ with amplitude 0.0374. This peak corresponds to the periodic behaviour of the

reattachment line, which is induced by the passage of the large-scale structures impinging upon the bounding walls. The overall picture thus presented from figures 3 and 4 is the one in which the interior shear layer is found 'flapping'. This 'flapping' process is related to the interaction of the vortical structures with the two vertical endwalls.

Figure 5 represents the streamwise velocity contours along with various axial cross-sections in the recirculation region at time $t = 10.35$ s. Figure 5(a) corresponds to the chosen axial cross-sections where the streamwise velocity contours are plotted. Figure 5(b) highlights the flow pattern, which is characterized by the strong streamwise vortices in the recirculation zone. The axial cross-section, a, adjacent to the step plane, shows the formation of the floor eddy. From the adjacent axial cross-section, b, it is understood that this eddy bulged and started to interrupt the downstream flow. This shedding eddy induced a shear layer between the recirculation region and the upstream flow. Also, this shedding eddy was responsible for the induction of the Kelvin–Helmholtz instability that is discussed in depth in § 4.3. In the subsequent cross-sectional plane, c, the size of this shedding eddy was seen to be reduced and in contrast the formation of roof eddies was observed in the vicinity of the endwalls. The axial cutting plane, d, shows the disappearance of floor eddy, reduction of roof eddy and constant flow separation. In the reattachment region, the eddy formation was due to pressure reduction. The decreased pressure was caused by the presence of the step that induced the sudden expansion of the upstream flow. This phenomenon, however, usually occurs at a location downstream of the step.

Figure 6 highlights the three-dimensional structure of the recirculation regions close to the vertical endwalls and step wall. In addition, the streamwise velocity contours are plotted at the translucent symmetry plane at time $t = 10.35$ s. The streamwise iso-contours clearly show the strong three-dimensionality of the flow involving a wall jet at the step plane and the complex vortex structures. From figure 6, it can be observed that the vortical structures extend well into the upper and lower corners of the channel downstream and also into the central flow field. Similar observations were also acknowledged by Williams & Baker (1997). The formation of the recirculation region and its role as a barrier for the upstream flow are explained below. The shedding-eddy formation is clearly visible near the step wall. At an early stage, the recirculation region was found in the vicinity of the step wall, two vertical endwalls and channel floor, but not the channel roof. As time elapsed, the size of the recirculation region increased. Owing to the increase of size of the recirculation region, the rate of pressure recovery was liable to decrease. This process led to an incipient separation on the roof owing to the decreased adverse pressure gradient. After a while, the recirculation region acted as a barrier for the upstream flow (figure 6). Beyond the reattachment, the flow recovered progressively towards a fully developed state. Another predominant feature observed within the recirculation zone was the substantial increase in the transitional activity. This phenomenon was due to the formation of significant unsteady features occurring below the interior 'flapping' shear layer.

The 'flapping' motion in the reattachment region was promoted by shear-layer instability and shedding-type instability. While the former instability mode corresponds to the natural roll-up process of the shear layer, the latter corresponds to the interaction of the entire shear layer with the wall. The shedding-type instability was directly related to the formation of the large vortical structure (the hairpin-like vortex tube). The roll-up process of the shear layer had been regarded as a potential 'amplifier' for the vortical structures. The moment when the disturbance was amplified

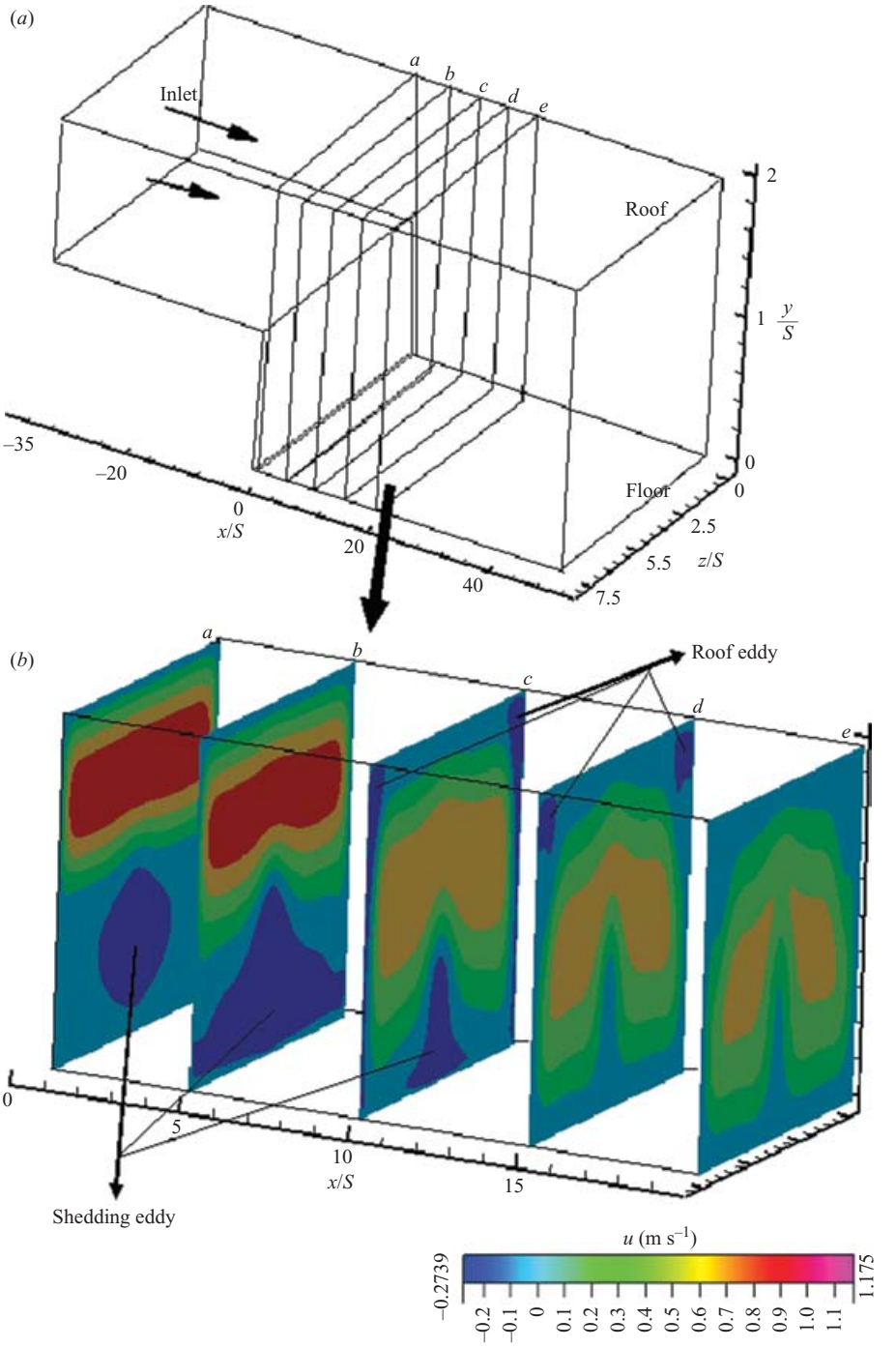

FIGURE 5. The simulated streamwise velocity ($u\,(\mathrm{m\,s^{-1}})$) contours at various axial locations ($a\,(x/S=1)$, $b\,(x/S=5)$, $c\,(x/S=10)$, $d\,(x/S=15)$ and $e\,(x/S=20)$) for illustrating the formation of the shedding eddy and roof eddy at an instantaneous $t=10.35\,\mathrm{s}$. Arrows in (a) indicate the flow direction.

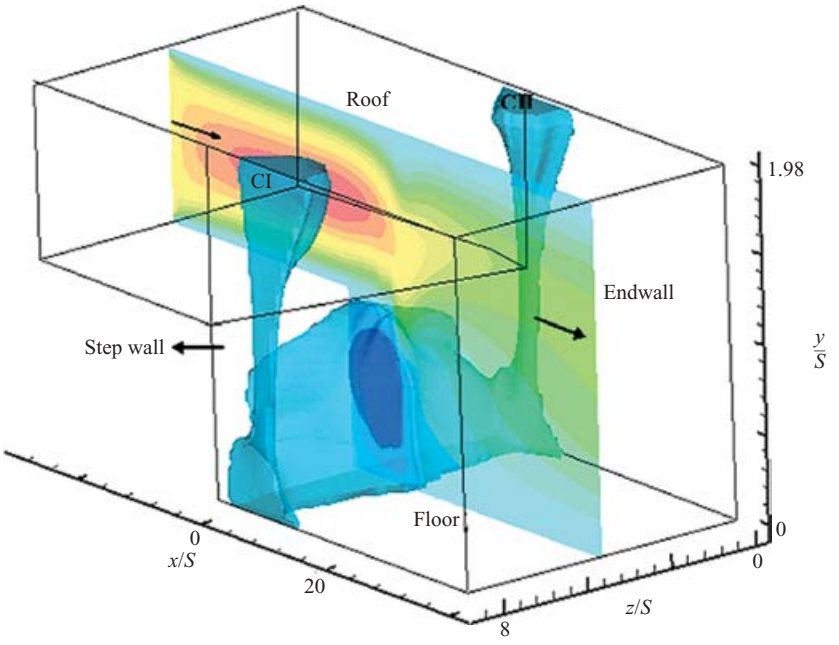

FIGURE 6. The simulated streamwise velocity iso-contours at $t = 10.35$ s along the translucent symmetry plane ($z/S = 4$) (showing the shedding eddy near the step wall) and recirculation regions (CI, CII) (near the vertical endwalls). (Colour gradation is shown in figure 5.)

by the shear layer, the large vortical structures were seen to grow faster and interact earlier with the wall, thus promoting flow reattachment considerably. These two instabilities are discussed in §§ 4.3 and 4.4.

4.2. *Flow topology*

In this section, the recirculation region was analysed with the help of the simulated streamline portrait. The support for the proposed streamline portrait was provided in two ways: (i) by invoking the topological constraints and structural stability criteria; and (ii) by listing the corroborative experimental evidence.

4.2.1. *Streamline portrait*

As proposed by Mackay (1994) and Raguin & Georgiadis (2004), the simulated streamfunction of the stationary helical vortex (SHV) allowed us to construct a streamline portrait of the flow or flow skeleton. This map containing the critical points and the limiting fluid particle trajectories could well characterize the flow. The SHV flow skeleton is presented as an (x, z) projection adjacent to the roof plane ($y/S = 1.979$) and an (x, y) projection of the spanwise symmetry plane ($z/S = 4$) in figures 7(a) and 7(b), respectively. These figures represent the cross-sections of the three-dimensional streamfunctions that correspond to the transverse cuts of the three-dimensional stream tubes. The SHV flow pattern is equivalent to the mapping of the three-dimensional trajectories of the fluid particles to the reduced coordinate systems. Mathematically speaking, the fluid trajectories are merely the fibres in the flow domain that constitutes a local vector bundle (Abraham, Marsden & Ratiu 1988) whose projection is shown in figure 7.

From figure 7(a), it is observed that on the channel roof there exist two recirculating cells, which are clearly delineated. Each of them has an elliptic point at its centre,

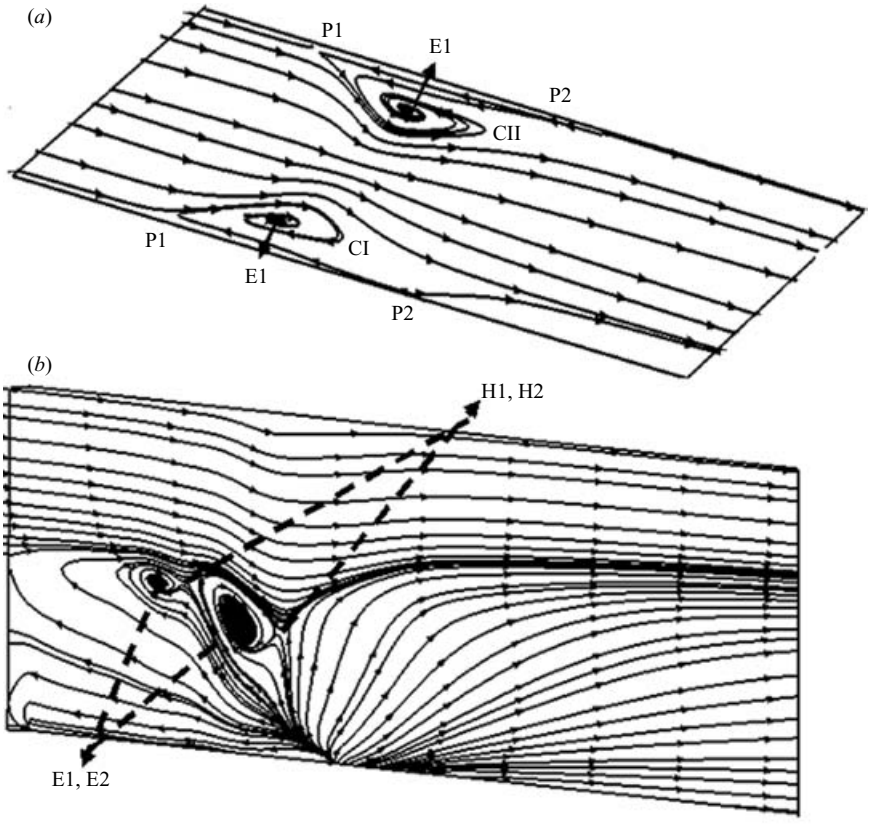

FIGURE 7. At $t = 10.35$ s, the simulated streamlines and critical points (a) on the roof ($y/S = 1.979$) consist of two regions CI, CII; (b) at the symmetry plane ($z/S = 4$), where E, H and P denote the elliptic, hyperbolic and parabolic points, respectively.

corresponding to the two counter-rotating helical vortices in the double helix topology. In figure 7(a), the counter-rotating cell enclosing the elliptic point E1 is labelled as CI while the co-rotating cell enclosing the elliptic point E2 is denoted as CII. Owing to the symmetry of the flow, the sizes of the two vortices CI and CII are seen to be equal. Each elliptic point E1 and E2 was bounded by a pair of parabolic points (P1, P2). The symmetry plane shown in figure 7(b) indicates that the recirculating cells are separated by an elliptic point in its centre. In addition to the elliptic points, two more critical points, namely, the hyperbolic points H1 and H2, are seen on the symmetry plane.

The three-dimensional flow structure of the SHV is shown in figure 8, in which a few iso-contours of the streamfunction (or stream tubes) are plotted. The transverse sections of the streamfunction are also represented in order to elucidate the topology of the streamfunction. Figure 8 also focuses on the two counter-rotating helical vortices. Since the flow pattern is shown at a particular time, the streamlines and fluid particle trajectories remain identical. A particle trajectory on one of the stream tubes shown in figure 8 clearly indicates the presence of the double helix pattern. This helix-flow nature was found to originate from the vertical endwall and travelled in a spanwise direction as vertical rollers until it reached the symmetry plane. The velocity distortion near the step and the presence of a shedding eddy in the recirculation region

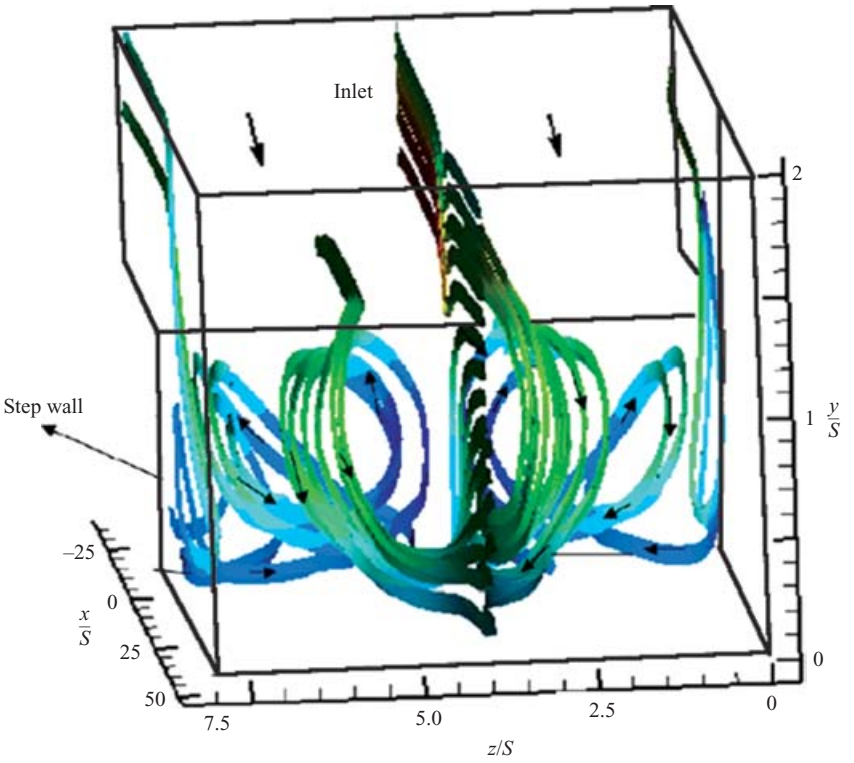

FIGURE 8. The simulated stream tubes at $t = 10.35$ s (the colour gradation is shown in figure 5). Arrows indicate the flow direction. The stream tubes appear as vertical rollers and form the double helix pattern.

were responsible for these helix flows. It was observed that outside of the recirculation region, the streamlines formed a straight-line pattern parallel to the vertical endwalls with the disappearance of the helix pattern (figure 8).

4.2.2. *Corroborative evidence for the simulated SHV streamline portrait*

Now we understand that the streamline portrait in figure 7 is realistic. The simplest topology constraint is based on the Euler number ξ of the flow. As explained by Jana, Metacalfe & Ottino (1994), the Euler number on a surface is defined as the sum of the Poincaré indices of the critical points on the surface. The Poincaré index of a hyperbolic point is -1, a parabolic point is $-1/2$, and for an elliptic point it is 1. The topological invariance relation is given by

$$NE - \left(NH + \tfrac{1}{2}NP\right) = \xi = 0, \tag{3}$$

where the NE, NH and NP represent the number of elliptic points, hyperbolic points and parabolic points, respectively. While the topological relation given in equation (3) itself does not guarantee the existence of the flow, it is customary to consider it as a way to check the topological consistency. Obviously, the SHV streamline portrait, exhibited on the channel roof in figure 7(*a*), satisfied the topological rule given in equation (3) as $NE = 2$, $NH = 0$ and $NP = 4$. Similarly, the critical points on the plane of symmetry (figure 7*b*) are distributed in a way that satisfies equation (3) with $NE = 2$, $NH = 2$ and $NP = 0$. Though we could validate the simulated SHV velocity field by pursuing the idea that the physically realizable kinematics of a flow

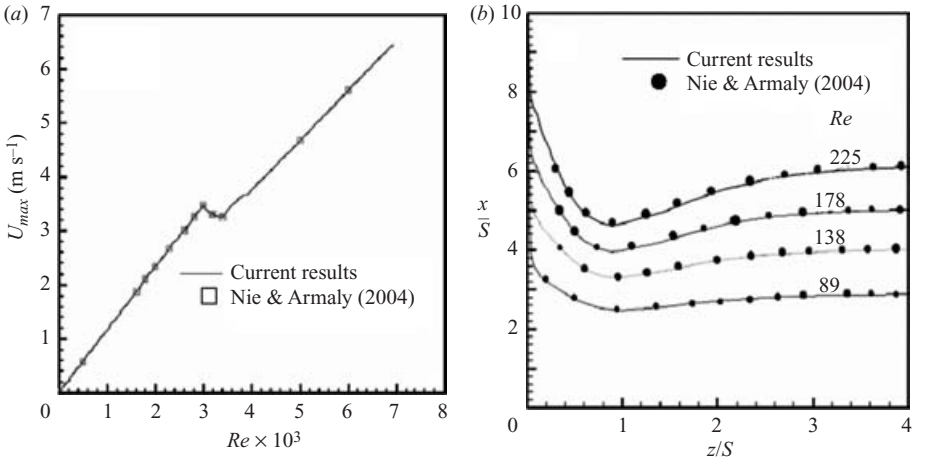

FIGURE 9. (*a*) Plot of the mean streamwise velocity component at the centreline of the inlet duct at $x/S = -1$ and $y/S = 1.49$. (*b*) A comparison of the measured and the currently simulated zero shear stress lines at $y/S = 0.05$.

was related to its stability, we focused only on the structural stability of the SHV mode, however, subjected to the infinitesimal changes to the geometry and boundary conditions in the currently investigated system. Drazin & Reid (1981) defined a structurally stable system as one which did not change in the qualitative character of its solution(s) under the infinitesimal changes of the geometrical and physical parameters of the problem, fluid properties and boundary conditions. The SHV flows depicted in figures 7 and 8 are structurally stable according to theorem (3.2) in Ma & Wang (2001). Indeed, their conditions for the structural stability criteria of the divergence-free vector fields that satisfy the Dirichlet boundary conditions (no slip at the walls) are met. The velocity field is sufficiently regular and a parabolic point on the boundary is connected to another parabolic point on the same boundary (in figure 7*a*, P1 is connected to P2 and they are located on the same endwall). The two parabolic points, P1 and P2 shown in figure 7(*a*), are connected with the stable manifolds. These manifolds corresponded to the flow regions CI and CII, which are separated by the counter-rotating cells. These manifolds acted as barriers for the two vortices (E1, E2) when the flow was observed from the inlet. In order to verify whether the flow structure was structurally stable, we had to further corroborate the fidelity of the reconstruction of the SHV velocity field from the experiments.

The mean streamwise velocity components at $(x/S, y/S, z/S) = (-1, 1.49, 4)$ for the various Re values were plotted and compared with the experimental results of Nie & Armaly (2004) that are shown in figure 9(*a*). Figure 9(*a*) shows clearly the flow transition development from the laminar to turbulent region, which occurs in the upstream section of the step ($x/S = -1$, $y/S = 1.49$ and $z/S = 4$). The centreline streamwise velocity component in the transition flow regime ($Re = 3300 - 4500$) remains approximately constant. This is due to the changes developed in the velocity distribution in this flow range (Nie & Armaly 2004). Otherwise, the streamwise velocity component in this upstream section of the step appeared to be proportional to the Re in both the fully laminar and turbulent flow regimes. The spanwise distribution of the zero shear stress lines on a plane adjacent to the step wall ($y/S = 0.05$) is shown in figure 9(*b*) in line with the results of Nie & Armaly (2004). Excellent agreement has been found between the present computational and the referenced experimental

results (Nie & Armaly 2004). Figure 9(*b*) indicates the reverse flow regions bounded by zero shear stress lines, which increase in size and move further downstream as the *Re* increases in the laminar flow regime.

4.3. *Existence of Kelvin–Helmholtz (shear-layer) instability*

In this section, an attempt is made to understand the Kelvin–Helmholtz instability with the aid of the simulated streamline topology in the backward-facing step flow. In figures 10(*a*) and 10(*b*), the side view and front view of the streamwise velocity iso-contours are shown. The recirculation regions, which are clearly delineated from the upstream flow, are also seen. The highlighted wavy region in the front view of figure 10(*b*) confirmed the developed Kelvin–Helmholtz instability. Figure 10(*c*) depicts the streamlines and axial velocity vectors on the plane of symmetry ($z/S = 4$) in order to reveal the complex interaction near the step. The upstream flow was divided into two separate flow regions in the recirculation zone and these regions interacted with each other at the symmetry plane. This resulted in the formation of an unstable interior axial shear layer (figure 10*d*) that had a wavy appearance. Two incipient loop-like vortices that are seen below the interior shear layer (figure 10*c*) hereinafter referred to as hovering vortices, wrap around the shedding eddy (figure 10*c*). The existence of a pair of spiral nodes and the saddles in figure 10(*c*) indicated the growth of Kelvin–Helmholtz-like shear-layer instability near the step wall region. Flow instability of this type would, however, cause the pitchfork bifurcation to occur. These initially tilted vortices were gradually convected upward alongside the flow to join a large-scale vortical roll-up process. The Kelvin–Helmholtz-like vortices were noticed only at the recirculation region (figure 10*b*, *c*). The three-dimensional view of the axial velocity contours, shown in figure 10(*c*), demonstrates the presence of such roll-up Kelvin–Helmholtz vortices. Again, figure 10(*c*) clearly exhibits a train of instability-induced shear-layer rollers alongside the symmetry plane of the backward-facing step. However, because of the transitional flow behaviour at $Re = 900$, the vortices were bound to lose their strength at a fast rate while approaching the downstream side of the step. On the other hand, we could easily infer from figures 10(*b*) and 10(*c*) that even the wavy (unstable) character had its role in contributing to the formation of the relatively weaker Kelvin–Helmholtz vortices. Similarly, such Kelvin–Helmholtz instability was predicted numerically by Delcayre & Lesieur (1997).

As far as the three-dimensional evolutional details of the Kelvin–Helmholtz vortices are concerned, it is worth mentioning that many researchers presumed that the Kelvin–Helmholtz vortices grew in the form of closed-loop (ring-like) structures, with the downstream part of such rings remaining tilted upward. Figure 8 clearly shows that the Kelvin–Helmholtz vortices did not form closed vortex rings. Rather, in the recirculation region, they appeared in the form of vertical rollers. The two arms of the rollers joined the locally evolving counter-rotating vortex pair (CVP) while approaching the symmetry plane. The growth of the CVP from the lateral sidewall shear layers prevented the formation of a closed-form vortex ring by the extended Kelvin–Helmholtz rollers. In order to emphasize this point, in figure 10(*d*) we have

FIGURE 10. The simulated iso-contours at $t = 10.35$ s of the axial velocity and streamlines for revealing the growth of Kelvin–Helmholtz (K-H) instability. (*a*) Side view (R indicates recirculation region). (*b*) Front view (translucent region denotes the normal flow region) for showing the K-H flow instability (highlighted in rectangle). (*c*) The simulated streamlines, spiral nodes (◆) and the saddles (×) on the symmetry plane $z/S = 4$. (*d*) Axial velocity vectors along with the interior shear layer and eddies. (Colour gradation is shown in figure 5.)

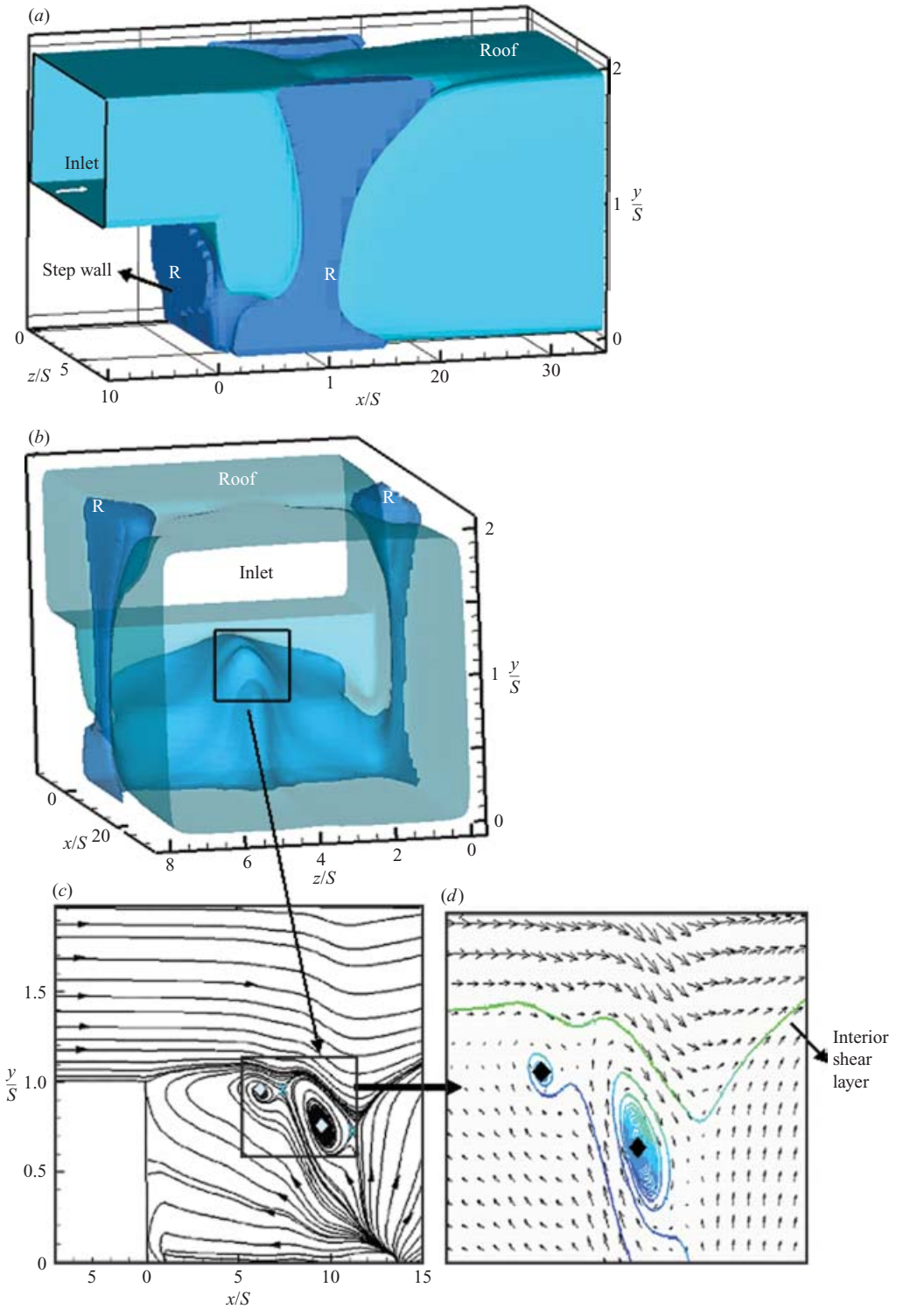

FIGURE 10. For caption see facing page.

presented a sectional view of the axial velocity contours on the symmetry plane $z/S = 4$. Similar vortical flow development was also seen to take place on different closely placed (x, y)-planes about the symmetry plane. In fact, the sectional axial velocity contours near the vertical endwalls did not show any indication of the presence of Kelvin–Helmholtz rollers. (However, we do not present these sectional contours to conserve space.) This Kelvin–Helmholtz instability corresponds to the natural roll-up process of the shear layer. The interaction of the entire shear layer with the bounding wall corresponds, however, to the shedding type instability that led the formation of large vortical structures.

4.4. *Vortex structure distortion in the recirculation zone*

An attempt was made, with the aid of a simulated velocity field, to visualize the structure of the vorticity field. The predicted three-dimensional coherent structures such as vortex lines, vortical corelines and vortex tubes that formed in the very high topologically complex recirculation regions were analysed. The present fully developed backward-facing step flow that contains organized vortex tubes (also called vortex filaments or 'worms') was advected homogeneously and isotropically by the velocity field (Vincent & Meneguzzi 1994). Generally, the vortex tubes, which are the locally quasi-steady solutions of the Euler equations, occur in regions where the nonlinearity is depleted. The vorticity field indeed tended to be more entangled in the topologically complex recirculation regions, although it was found that the vorticity field of this homogeneous flow was complicated everywhere. The correlation between the topological complexity and the recirculation regions for the $Re = 900$ case revealed that the viscous diffusion of vorticity was not very strong in these recirculation regions. Hence the existence of sufficiently well-defined vortical structures was seen in this region. These vortical structures are, however, associated with the 'flapping' vortices (figure 3). What was observed primarily was the high strain rates generated between the 'flapping' vortices that enhanced the momentum transport. Further, the development and deformation of spanwise coherent vortices were understood. To visualize these vorticity distortions, the vortex lines (material lines) were selected in the downstream part of the backward-facing step at planes parallel to the transverse and spanwise directions at various axial locations in the subsequent analysis.

The streamwise vortex's stretching and rolling-up natures have been highlighted using a single streamwise vortex line of finite width along with the axial cross-sectional $(x/S = 7)$ velocity contours (figure 11). This picture explicitly reveals the shedding eddy in the vicinity of the floor and the shear layer. The path of the vortex line has been found in between the shear layer with the high degree of nonlinearity. It was observed that whenever the recirculation occurred in the downstream owing to the formation of eddies, the trail of the vortex line surrounded the floor eddy and thus formed a closed loop. The spirally prolonged or stretched vorticity nature was also seen near the roof eddies, but this spiral vorticity nature did not show symmetric behaviour. Again, the figure shows that the vortex lines are lifted up by the floor eddy. From the above observations, it was concluded that, in the recirculation region, the floor eddy and the vortex lines were strongly correlated.

The three-dimensional top view of vortex lines in figure 12(a) demonstrates the spanwise vortex columns configured in the staggered row. These columns were generated by the shear-layer instability (Kelvin–Helmhotz instability). The disturbances of the separated shear layer at the flank of the step plane, however, grew towards the downstream direction in order to corrugate the layer in the spanwise direction. This process triggered the three-dimensional deformation of the spanwise vortices and

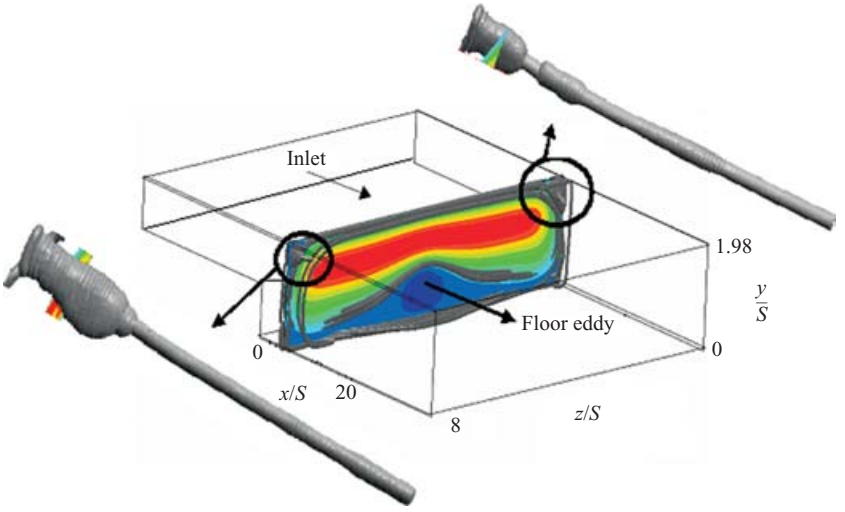

FIGURE 11. The simulated axial streamwise velocity contours at $x/S = 7$ (colour gradation is shown in figure 5) and $t = 10.35$ s for depicting the eddy formation near the floor and a stretched vortex line for depicting the stretching and rolling-up vortical flow feature near the roof eddies (highlighted in a circle).

also the final formation of the staggered array of quasi-streamwise vortices. Similar predictions have also been observed by Yanase *et al.* (2002). Figures 12(*b*) and 12(*c*) depict the streamwise stretching value ($= (\overline{\omega} \circ \nabla)\overline{V}$) with respect to time at the locations (17, 1.975, 5×10^{-5}) and (8, 1, 4). The stretching value near the endwalls rose slowly and attained a peak, then decreased and remained as a steady-state value. It was observed that at about 5 s, the streamwise vorticity converges to zero value and hence the stretching parameter values go to zero at about 5 s (figure 13). The stretching value was large near the vertical endwalls compared to the centreplane. Apart from that, the stretching values had a stronger oscillatory behaviour in the centreplane compared to those of the vertical endwalls. This oscillatory behaviour was the direct consequence of the flapping motion of the interior shear layer. From a physical point of view, this implies that a fluid element would first contract in the direction perpendicular to the vorticity vector, and then stretch along this direction in order for the angular momentum to be conserved (if dissipation is neglected). The vortex-stretching mechanism is held responsible for the local amplification of the vorticity magnitude and thus for the production of smaller- and smaller-scale structures in the flow field. This phenomenon thus implies a transfer of energy from large length scales to smaller ones, usually known as the energy cascade (Guermond, Oden & Prudhomme 2004).

The stretching and rolling-up natures of a single vortex line in the separation and reattachment region are highlighted in figure 13. Figure 13 also shows the typical time series of a partial streamwise vortex line (in the colour gradation of ω_x) on the two-dimensional (x, z)-plane. This vortex line was chosen in the vicinity of the floor ($y/S = 1 \times 10^{-20}$) and in regions parallel to the step wall at $x/S = 6.48$. A reference line of the flow separation (blue in colour) was superimposed over the vortex line. The red-coloured vortex line represents the positive vorticity whereas the blue colour the negative. In the first instance (figure 13*a*), when the flow passed over the step (at $x/S = 0$), the separation line was evident and a straight vortex line was seen. At a later time $t = 0.2$ s, this vortex line was seen to roll-up (figure 13*b*) in a clockwise

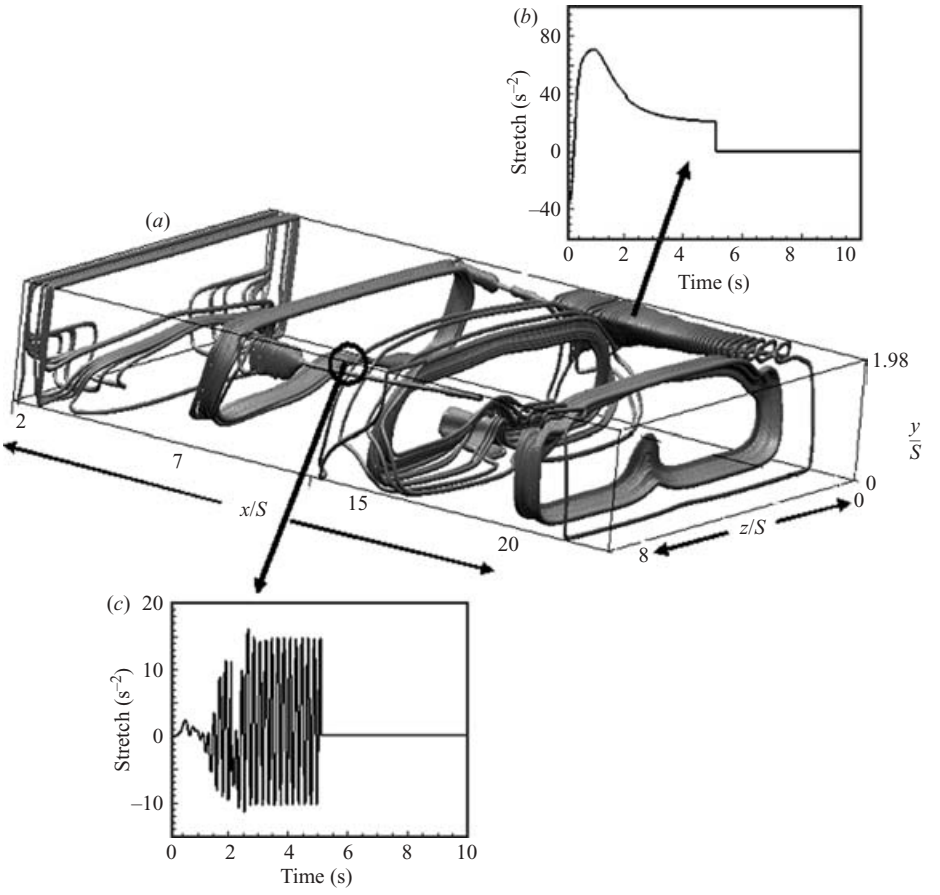

FIGURE 12. The simulated streamwise vortex lines and their stretching values at the chosen locations. (*a*) Streamwise vortex lines at various chosen axial locations along the downstream at $t = 10.35$ s to highlight the stretched and spiralled nature of the vortex lines. (*b*, *c*) The streamwise stretching values with respect to time at two locations (17, 1.975, 5×10^{-5}) and (8, 1, 4), which are highlighted in (*a*).

direction. It was evident that the shear-type and shedding-type instability induced distortions. As a result, this vortex line was stretched in the spanwise direction (figure 13*c*). After a few seconds, i.e. at $t = 2$ (s), the vortex line became small in size and weak in vortex strength and started to stretch and roll-up (figure 13*d*). In the next instance (figure 13*e*), the vortex head was seen to be fully rolled up and it began to grow larger and stronger. In the subsequent instance (figure 13*f*), it was stretched in between the two vertical endwalls and elongated in the streamwise direction. Also, this vortex line continued to rise in the transverse direction. All these behaviours led us to conclude that the vortex lines underwent severe deformation in the recirculation region through the instabilities and self-destructive interactions.

4.5. *Formation of lambda* (Λ)*, hairpin-like and vertical endwall vortices*

As discussed earlier, the important mechanism affecting the reattachment process was the formation of vortical structures and their interaction with the bounding walls. The vortical corelines and vortex tubes found in the recirculation zone are shown in figure 14. According to Robinson (1989), 'A vortex exists when instantaneous

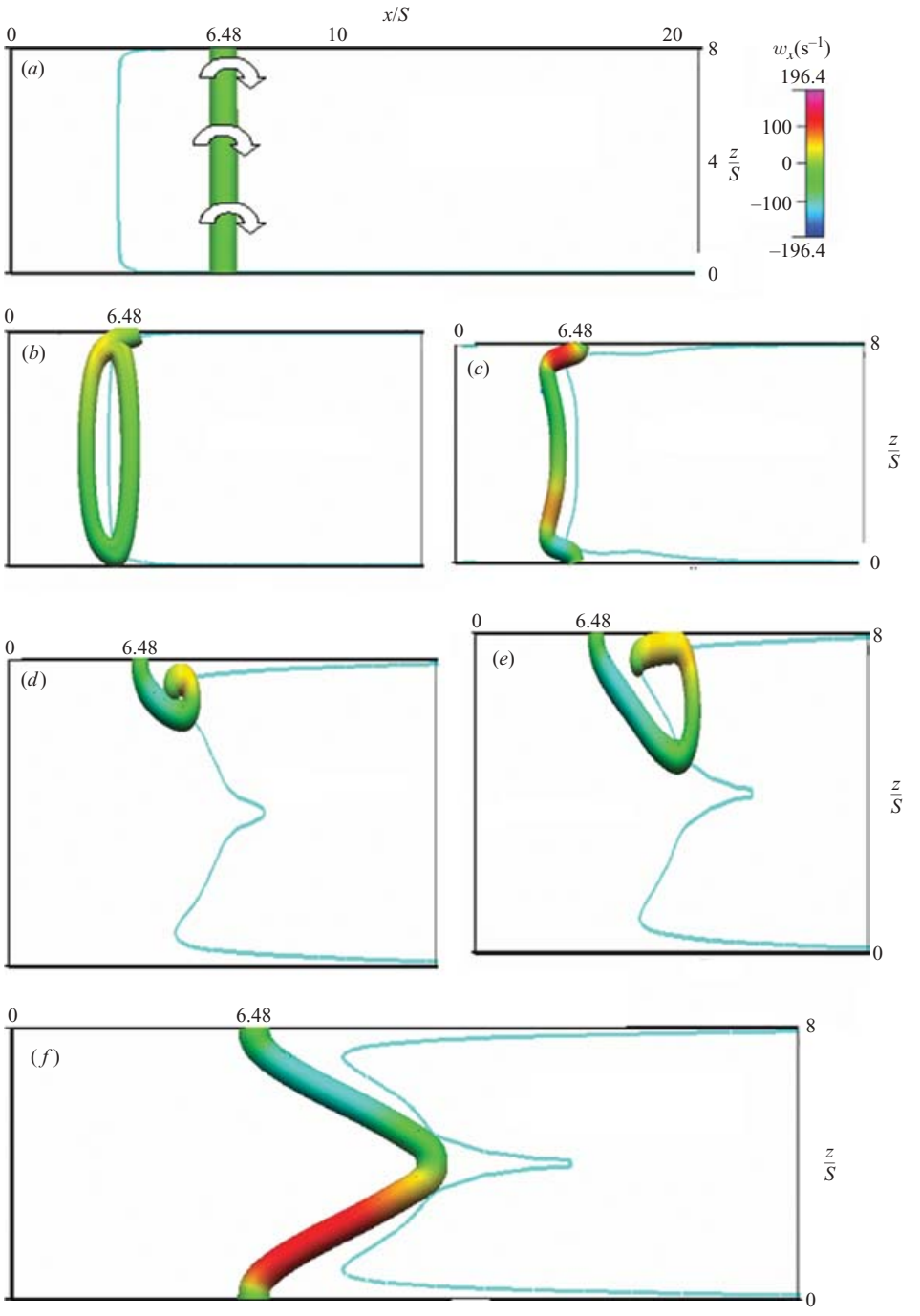

FIGURE 13. The simulated vortex line with the amplified finite width at (6.48, 1×10^{-20}, 7.93) in the colour contours of the streamwise vorticity vector (ω_x) along with the line of separation (blue) at (*a*) $t = 0.1$ s; (*b*) 0.2; (*c*) 0.4; (*d*) 2; (*e*) 3; (*f*) 3.09 s. times.

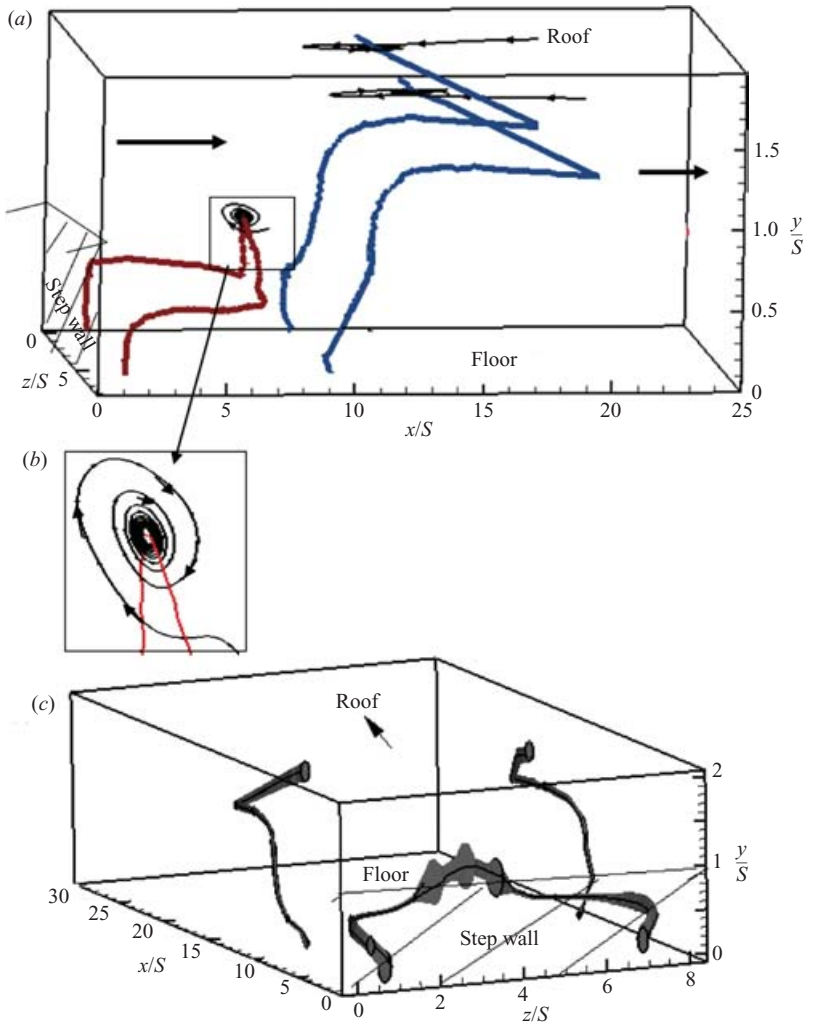

FIGURE 14. (*a*) The simulated vortical corelines (in red, the hairpin vortical structure; blue, the vertical endwall vortical structures) at $t = 10.35$ s, (*b*) spiralling nature of the streamlines (black) around the vortical coreline (red) and (*c*) the simulated vortex tubes present in regions downstream of the backward-facing step. Arrows indicate the flow directions.

streamlines mapped onto a plane normal to the vortex core exhibit a roughly circular or spiral pattern, when viewed from a reference frame moving with a centre of the vortex core' (figure 14*a*,*b*). These vortical corelines were extracted based on the velocity gradient eigenmodes. The vortex tubes around the vortical corelines are drawn at the constant circulation $\Gamma = 1 \times 10^{-5}$. Figure 14(*a*) gives us an idea about the vortical coreline structures in the recirculation region. An important feature of this figure was its complex surface streaking pattern. The spiralling vortex motion had its origin in the bounding endwalls because the fluid particles near the endwall could cause the vortical flow to proceed along the third dimension. The global three-dimensional nature of the flow is best illustrated by the transverse vortex tube in figure 14(*c*). Fluid particles around this tube had the tendency to move spirally towards the plane of symmetry.

Figures 14(*a*) and 14(*c*) show the presence of two different vortical structures in the separation/reattachment region. One vortical coreline is emerging from the step wall and proceeding towards the downstream to form the hairpin-like structure. This vortex coreline is characterized by two quasi-streamwise legs lying on the floor close to the step wall and a hairpin loop. This hairpin-like vortical coreline formed a lambda-shaped structure around the unstable interior shear layer seen in figure 11(*d*). It can be seen that the cross-sectional area in the lambda-like vortex has a very low vorticity magnitude. In the hairpin-like vortex structure, this low vorticity had led to the larger surface area for the lambda-like vortex (figure 14*c*). Delcayre & Lesieur (1997) noticed the similar hairpin-like vortices in turbulent case with $Re = 5000$. They demonstrated that the transition towards turbulence was characterized by the transformation of spanwise vortices onto the streamwise vortices.

The other pair of vortical corelines was situated very close to the vertical endwalls in the recirculation region. They had their origin/end points at the roof/floor, respectively. These two symmetrical vortical lines were observed near the two recirculation regions of CI and CII that are shown in figure 6. A very strong predominant vorticity nature was found very close to the flanks of the vertical endwalls.

In considering the above observations, the results are summarized as follows:

1. While inspecting a huge amount of time-sequence numerical data taken in different regions of the backward-facing step channel, it was found that the vortex augmentation process was significant between $x/S = 10$ and $x/S = 20$ in the downstream side of the step. Results exhibited the generation of vortical structures in the recirculation region below the interior shear layer. These structures strongly interacted with the bounding walls and induced a 'flapping' motion of the whole shear layer.

2. The reattachment region in the backward-facing step flow was promoted by shear-layer instability and shedding-type instability. While the former instability mode corresponds to the natural roll-up process of the interior shear layer, the latter corresponds to the interaction of the entire shear layer with the bounding walls. The shedding instability was directly related to the large vortical structures (hairpin-like vortex tube and vertical end wall vortex tubes) and induced a 'flapping' motion.

3. From the streamwise perspective, the backward-facing step flow could cause localized rotation to develop on the flanks near the step wall via the tilting (and the subsequent stretching) of vortex lines associated with the strong shear flow. This flow had led to the development of significant dynamic pressure gradient forces on the flanks of the step wall and vertical endwalls. This dynamic forcing, which was significantly nonlinear, had led to the development of a correlation between the flow and the midlevel rotation. This nonlinear correlation, however, prompted the formation of vortex corelines near the vertical endwalls and close to the step wall.

4. The downstream side of the channel step had been classified into three regions: in regions close to the step ($x/S \leqslant 7$) the fluctuations were dominated by the quasi two-dimensional Kelvin–Helmholtz rollers; in the downstream regions ($1 \leqslant x/S \leqslant 7$), the rollers underwent strong three-dimensional contortions and appeared as lambda (Λ)-vortices. The fluctuations developed like hairpins (oriented with the head towards the high-momentum region). The Kelvin–Helmholtz vortices were turned into lambda (Λ) vortices which impinged on the wall and were elongated into the big arch-like (hairpin-like) vortices. Further downstream ($x/S \geqslant 10$), at about the attachment location in the flanks of the recirculation region, vertical endwall vortical structures were present.

5. Conclusions

Based on the direct numerical simulation results for the homogeneous isotropic flow over a backward-facing step, a detailed topological study and vortex analysis were carried out. The vorticity analysis of this flow problem had led us to propose a new scenario to explain the transitional cascade. The three-dimensional flow model undertaken consisted of an expansion ratio of 2.02 and a downstream aspect ratio 8. The results were validated by a streamline portrait of the flow. We had subsequently provided the support for the proposed streamline portrait in two ways: (i) by invoking the topological constraints and structural stability criteria; and (ii) by showing corroborative experimental evidence. A very good agreement was, however, found. A pair of counter-rotating helical cells configured in a double-helix structure wrapped around the vortex tubes was observed. The simulation supported by the simulated spectra provided evidence that the strong sensitivity of the flow in the recirculation zone was due to the perturbation-induced specific changes toward the evolution of the vortical structures within the separated interior shear layer. This event could enhance the flapping motion of the interior shear layer.

In the sudden expansion region near the step, the fluid elements in the vicinity of the sidewalls were engulfed in the primary recirculation. Then the fluid elements moved towards the channel mid-plane through the spiralling motion where they were eventually caught up in a predominantly two-dimensional recirculating flow and then exited the separation bubble into the main stream. Finally, they follow the straight-line path parallel to the vertical endwalls. The behaviour of the unstable interior shear layer was investigated at several planes in order to describe the primary instability (spanwise vortices) as well as the vortices transferred from the spanwise to the streamwise direction.

In the recirculation zone, it was observed that the vortex structures underwent stretching and rolling-up through the instabilities and self-destructive interactions. The simulated roll-up process of the shedding shear layer was manifested by the presence of hovering vortices, the topological saddle points and the Kelvin–Helmholtz-like vortices. The developed Kelvin–Helmholtz-like instability near the step wall interface was found to initiate the roll-up process of the downstream shear layer. Notably, the Kelvin–Helmholtz vortices did not form the closed vortex rings in the recirculation region, rather, their open tails were extended towards the centreplane.

The vortical corelines were observed around the shedding shear layer near the step wall and flanks of the vertical endwalls. The Kelvin–Helmholtz vortices were turned into hairpin-like vortices with two streamwise legs placed very close to the step wall. The shedding shear layer distorted this hairpin-like vortex tube and thus formed the lambda-shaped vortex structure near the centre plane. Another symmetrical pair of vortex tubes was also observed near the vertical endwalls whose origin/end was located on the channel roof/floor, respectively.

The financial support from the National Science Council, under NSC92-2218-E-002-026-YF, of Republic of China is gratefully acknowledged.

REFERENCES

Abraham, R., Marsden, J. E. & Ratiu, T. 1988 *Manifolds, Tensor Analysis, and Applications*, 2nd edn. Springer.

Armaly, B. F., Durst, F., Pereira, J. C. F. & Schonung, B. 1983 Experimental and theoretical investigation of backward-facing step flow. *J. Fluid. Mech.* **127**, 473–496.

Beaudoin, J., Cadot, O., Aider, J. & Wesfreid, J. 2004 Three-dimensional stationary flow over a backward-facing step. *Eur. J. Mech.* B/*Fluids* **23**, 147–155.

Choi, H., Hinze, M. & Kunisch, K. 1999 Instantaneous control of backward-facing step flows. *Appl. Numer. Maths* **31,** 133–158.

Drazin, P. G. & Reid, W. H. 1981 *Hydrodynamic Stability*. Cambridge University Press.

Dejoan, A. & Leschziner, M. A. 2004 Large eddy simulation of periodically perturbed separated flow over a backward-facing step. *Intl J. Heat Fluid flow* **25**, 581–592.

Delcayre, M. & Lesieur, M. 1997 Topological feature in the reattachment region of a backward-facing step. *1st AFOSR Intl Conf. on DNS and LES, Ruston.*

Gallaire, F. 2002 Swirling Jet instabilities and vortex breakdown control. PhD thesis, Ecole Polytechnique, Palaiseau, France.

Guermond, J.-L. Oden, J. T. & Prudhomme, S. 2004 Mathematical perspectives on large eddy simulation models for turbulent flows. *J. Math. Fluid Mech.* **6**, 194–248.

Guerrero, J. S. P. & Cotta, R. M. 1996 Benchmark integral transform results for flow over a backward-facing step. *Comput. Fluids* **25**, 527–540.

Gupta, A. K., Lilley, D. G. & Syred, N. 1984 *Swirl Flows*. Abacus, London.

Husan, M. A. Z. 1992 The flow over a backward-facing step under controlled perturbation: laminar separation. *J. Fluid Mech.* **238**, 73–96.

Jana, S. C., Metcalfe, G. & Ottino, J. M. 1994 Experimental and computational studies of mixing in complex Stokes flows: the vortex mixing flow and multicellular cavity flows. *J. Fluid Mech.* **269**, 199–246.

Jeong, J., Hussain, F., Schoppra, W. & Kim, J. 1997 Coherent structures near the wall in a turbulent channel flow. *J. Fluid Mech.* **332**, 185–214.

Kiya, M. & Sasaki, K. 1985 Structure of large-scale vortices and unsteady reverse flow in the reattaching zone of a turbulent separation bubble. *J. Fluid Mech.* **154**, 463–491.

Kiya, M., Shimizu, M., Mochizuki, O. 1997 Sinusoidal forcing of a turbulent separation bubble. *J. Fluid Mech.* **342**, 119–139.

Kosma, Z. 2000 Computing laminar incompressible flows over a backward-facing step using Newton iterations. *Mech. Res. Commun.* **27**, 235–240.

Koutmos, P. & Mavridis, C. 1997 A computational investigation of unsteady separated flow. *Intl J. Heat Fluid Flow* **18**, 297–306.

Lee, T., Huteau, F. & Mateescu, D. 2000 Flow past a 2-D backward-facing step with an oscillating wall. *J. Fluids Struct.* **14**, 691–696.

MA, T. & Wang, S. 2001 Structure of 2D incompressible flows with the Dirichlet boundary conditions. *Discrete Contin. Dyn. Syst.* B **1**, 29–41.

Mackay, R. S. 1994 Transport in 3D volume-preserving flows. *J. Nonlinear Sci.* **4**, 329–354.

Majda, A. 1991 Vorticity, turbulence, and acoustics in fluid flow. *SIAM Rev.* **33**, 349–355.

Nie, J. H. & Armaly, B. F. 2004 Reverse flow regions in three-dimensional backward-facing step flow. *Intl J. Heat Mass Transfer* **47**, 4713–4720.

Pierrehumbert, R.T. & Windal, S. E. 1982 The two and three dimensional instabilities for a spatially periodic shear layer. *J. Fluid Mech.* **114**, 59–82.

Raguin, L. G. & Georgiadis, J. G. 2004 Kinematics of the stationary helical vortex mode in Taylor–Couette–Poiseuille Flow. *J. Fluid Mech.* **516**, 125–154.

Robinson, S. K. 1989 A review of vortex structures and associated coherent motions in turbulent boundary layers. *Proc. 2nd IUTAM Symp. Struct. Turbul. Drag Reduct.* Zurich.

Vincent, A. & Meneguzzi, M. 1994 The dynamics of vorticity tubes in homogeneous turbulence, *J. Fluid Mech.* **258**, 245–254.

Williams, P. T. & Baker, A. J. 1997 Numerical simulations of laminar flow over a 3D Backward-facing step. *Intl J. Num. Methods Fluids* **24**, 1159–1183.

Yanase, S., Kawahare, G. & Kiyama, H. 2001 Three dimensional vortical structures of a backward facing step at moderate Reynolds numbers. *J. Phys. Soc. Japan* **70**, 3550–3555.

Yanase, S., Kawahara, G. & Kiyama, H. 2002 Evolution of three dimensionality in backward facing step flow at moderate Reynolds numbers. *Comput. Fluid Dyn. J.* **11**, 208–212.

Zhou, H. 1997 On the motion of slender vortex filaments. *Phys. Fluids* **9**, 970–981.